7-9-2012

Role of Self-Assembled Monolayer Passivation in Electrical Transport Properties and Flicker Noise of Nanowire Transistors

Seongmin Kim
Purdue University, kim482@purdue.edu

Patrick D. Carpenter
Purdue University, pdcarpen@purdue.edu

Rand K. Jean
Purdue University, rjean@purdue.edu

Haitian Chen
University of Southern California, haitianc@usc.edu

Chongwu Zhou
University of Southern California, chongwuz@usc.edu

See next page for additional authors

Kim, Seongmin; Carpenter, Patrick D.; Jean, Rand K.; Chen, Haitian; Zhou, Chongwu; Ju, Sanghyun; and Janes, David B., "Role of Self-Assembled Monolayer Passivation in Electrical Transport Properties and Flicker Noise of Nanowire Transistors" (2012). *Birck and NCN Publications.* Paper 863.
http://dx.doi.org/10.1021/nn302484c

Role of Self-Assembled Monolayer Passivation in Electrical Transport Properties and Flicker Noise of Nanowire Transistors

Seongmin Kim,[†] Patrick D. Carpenter,[†] Rand K. Jean,[†] Haitian Chen,[‡] Chongwu Zhou,[‡] Sanghyun Ju,[§] and David B. Janes[†,*]

[†]School of Electrical and Computer Engineering and Birck Nanotechnology Center, Purdue University, West Lafayette, Indiana 47907, United States, [‡]Department of Electrical Engineering, University of Southern California, Los Angeles, California 90089, United States, and [§]Department of Physics, Kyonggi University, Suwon, Gyeonggi-Do 443-760, Republic of Korea

ABSTRACT Semiconductor nanowires have achieved great attention for integration in next-generation electronics. However, for nanowires with diameters comparable to the Debye length, which would generally be required for one-dimensional operation, surface states degrade the device performance and increase the low-frequency noise. In this study, single In_2O_3 nanowire transistors were fabricated and characterized before and after surface passivation with a self-assembled monolayer of 1-octadecanethiol (ODT). Electrical characterization of the transistors shows that device performance can be enhanced upon ODT passivation, exhibiting steep subthreshold slope (~64 mV/dec), near zero threshold voltage (~0.6 V), high mobility (~624 $cm^2/V \cdot s$), and high on-currents (~40 μA). X-ray photoelectron spectroscopy studies of the ODT-passivated nanowires indicate that the molecules are bound to In_2O_3 nanowires through the thiol linkages. Device simulations using a rectangular geometry to represent the nanowire indicate that the improvement in subthreshold slope and positive shift in threshold voltage can be explained in terms of reduced interface trap density and changes in fixed charge density. Flicker (low-frequency, 1/*f*) noise measurements show that the noise amplitude is reduced following passivation. The interface trap density before and after ODT passivation is profiled throughout the band gap energy using the subthreshold current–voltage characteristics and is compared to the values extracted from the low-frequency noise measurements. The results indicate that self-assembled monolayer passivation is a promising optimization technology for the realization of low-power, low-noise, and fast-switching applications such as logic, memory, and display circuitry.

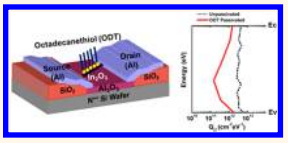

KEYWORDS: octadecanethiol · indium oxide · nanowires · flicker noise · transistor

Various types of semiconductor nanowires are considered to be promising candidates to extend the downscaling of complementary metal-oxide-semiconductor (CMOS) technology for future digital and analog electronics.[1] Nanowire transistors (NWTs) employing non-silicon materials can provide performance enhancements including large field-effect mobility (μ_{eff}) and high current drive suitable for integrating high-performance devices.[2−5] Among various nanowire materials, indium oxide (In_2O_3) is an attractive candidate for next-generation nanoelectronics because of its chemical stability, wide band gap, high μ_{eff}, compatibility with applications that require transparency and low-temperature processes, and its diverse applications in transistors, electro-optic devices, solar cells, and chemical/biosensors.[6−10] In particular, lightweight, optically transparent, and/or mechanically flexible thin-film transistors (TFTs) integrated with In_2O_3 nanowires and low-leakage high-*k* dielectrics on glass/plastic substrates have shown low threshold voltages (V_{th}) and high μ_{eff} compared to the amorphous-Si (α-Si), poly-Si, organic, or transparent conducting oxide (TCO) TFTs, which could enable future electro-optic applications such as heads-up/portable displays.[11] However, there are several issues to be resolved before manufacturing commercial products such as logic circuits and memory/display devices. Key challenges include integration of robust NWTs that provide stable device characteristics and low intrinsic noise. Also, high on-current (I_{on}), large μ_{eff}, high on/off current ratio (I_{on}/I_{off}), and small V_{th} near zero are required for high-performance and low-voltage operation. Furthermore, a steep subthreshold slope (SS) is required for large-scale digital application, in order to realize low-power operation. In displays, rapid switching is required for direct digital pixel driving, which can dramatically reduce the circuitry complexity.[12] However, due to the

* Address correspondence to janes@ecn.purdue.edu.

Received for review June 5, 2012 and accepted July 9, 2012.

Published online 10.1021/nn302484c

large surface-to-volume ratio of nanowires and the Debye length (λ_D), a measure of the field penetration into the bulk, which can be comparable to the nanowire diameter, the electronic properties of nanowire transistors are strongly influenced by the scattering from surface states. This can result in unstable and deteriorated device performance especially in terms of subthreshold current–voltage characteristics and noise spectra.[13] Therefore, in order to develop stable NWTs suitable for high-performance, low-power, and low-noise electronics, it is necessary to create high-quality interfaces along the body of the nanowire as well as the contacts. Many studies report that oxide semiconductor nanowires (or thin films) have a large amount of fixed charge states and interfacial traps, along with an electron accumulation layer at the surface.[5,11,14] Hence, most of the optimization techniques for semiconducting oxide NWTs to date have focused on controlling the amount of point defects such as O^-, O_2^-, OH^-, trap states, and donor-like oxygen vacancies at the nanowire surface.[6,15,16] However, such techniques often result in a nonpermanent change of the device behavior, and the exposed In interstitials at the nanowire surface yield a nanowire channel that is sensitive to ambient oxygen, suggesting that a proper passivation of the channel is necessary for enhanced and stable device operation. In such context, various studies have reported passivation of oxide nanowires within the NWT structure utilizing SiO_2, HfO_2, or organic layers such as polymethyl methacrylate (PMMA), which improves the device performance and stability.[12,17,18] However, such NWTs after passivation still exhibit high V_{th}, large SS, and low μ_{eff}, suggesting that further improvements are required.

Self-assembled monolayers (SAMs), ordered arrays of molecules with a hydrophilic headgroup at one end and hydrophobic tail groups at the other, have been widely used on nanoscale organic semiconductor hybrid devices since small molecules with diameters comparable to the atomic spacing can form a close-packed bonding structure to the nanowire surface.[19,20] Furthermore, there have been reports on utilizing fullerene-based SAMs to modify the surface properties of oxide thin films.[21] In this study, we have fabricated field-effect transistors (FETs) from individual In_2O_3 nanowires and shown that steep SS (~64 mV/dec) and near zero V_{th} (~0.6 V) along with high μ_{eff} (~624 $cm^2/V \cdot s$) and high I_{on} (~40 μA) can be realized when the nanowire channel is passivated with a SAM of 1-octadecanethiol (ODT). X-ray photoelectron spectroscopy (XPS) studies of the passivated nanowires indicate that ODT molecules are bound to In_2O_3 nanowires through the thiol linkages. Simulations using a two-dimensional device simulator (MEDICI) reveal that improvements in the device performance metrics after ODT passivation can be quantitatively analyzed in terms of reduction of interface trap densities and shifts in fixed charges. Low-frequency (flicker, 1/*f*) noise measurements in these devices show that the normalized noise spectrum and Hooge's constant are reduced following ODT passivation. Furthermore, the interface trap density profile at the energy band gap before and after passivation is extracted from the subthreshold current–voltage (*I*–*V*) curves and then compared with the values obtained from the 1/*f* noise measurements.

RESULTS AND DISCUSSION

The schematic diagram of a single In_2O_3 NWT device with individually addressable back-gate structure is shown in Figure 1. The NWTs consist of a heavily doped n^{++} Si as the back-gate, a patterned SiO_2 buffer layer, an atomic layer deposition (ALD)-derived Al_2O_3 gate insulator, a single-crystalline In_2O_3 nanowire for the channel,[22] and Al for the source–drain (S–D) electrodes. The inset of Figure 1d shows a field-emission scanning electron microscope (FE-SEM) image of a representative single nanowire bridging the gap between the source and drain electrodes. In order to improve device performance, previously reported optimization techniques were employed during the device fabrication steps. As shown in Figure 1, the nanowire at the contact regions was exposed to O_2 plasma (60 s) prior to S–D deposition, followed by a postmetallization ozone treatment (2 min) at the opened nanowire channel region and selective contact annealing (femtosecond laser fluence ~0.60 J/cm^2) at the contact region.[11,23,24]

Following device fabrication and post-treatments, the In_2O_3 nanowires within the NWT structure were passivated with ODT using the following procedure. The device wafer was rinsed in deionized (DI) water, dipped in anhydrous ethanol, and then immediately immersed in a 5 mM ODT solution in ethanol and transferred into a nitrogen-purged glovebox (O_2 < 5 ppm). After 8 h incubation in the solution at 70 °C, the wafer was removed from the solution, rinsed with ethanol, dried with N_2, and removed from the glovebox for immediate characterization. Nanowires for XPS characterization were prepared with the same process, but without removing the wires from the growth substrate, resulting in a dense multilayer mat of nanowires.

Nanowires before and after ODT passivation were characterized by XPS using a Kratos Axis Ultra DLD spectrometer with monochromatic Al Kα radiation ($h\nu$ = 1486.6 eV) at constant analyzer pass energy of 20 eV for high-resolution spectra and 160 eV for survey spectra. Spectra for the core levels of In 3d, C 1s, Si 2p, S 2p, and O 1s were taken at a photoemission angle of 0° and measured at high resolution to determine atomic concentration of the near-surface region and chemical state of the elements. The samples were mounted using a double-sided Cu tape and had good conductivity,

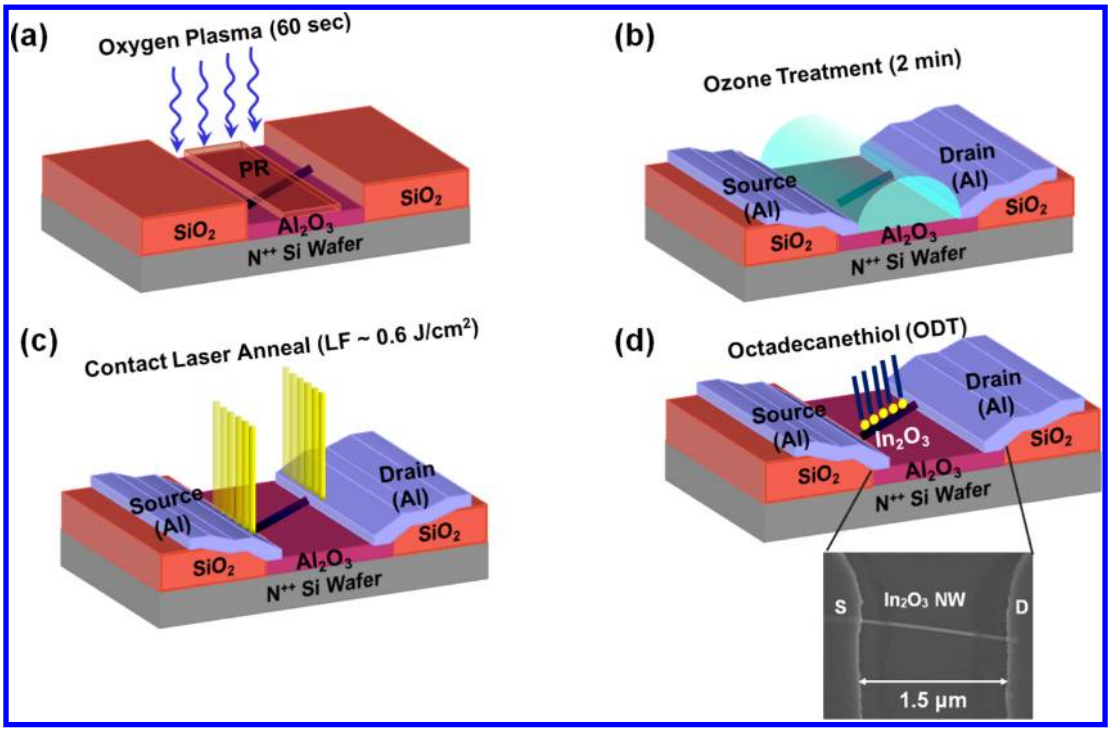

Figure 1. Schematic diagram of single In_2O_3 NWTs. In order to optimize the device characteristics, (a) the source–drain areas of the nanowire are exposed to oxygen plasma for 60 s prior to metallization, followed by postmetallization optimization techniques such as (b) ozone treatment (2 min) of the channel and (c) selective contact annealing using femtosecond laser (laser fluence ~0.60 J/cm^2). Finally, (d) passivation of the nanowire channel with a self-assembled monolayer of ODT. The inset shows the top-view FE-SEM image of a single In_2O_3 nanowire bridging the source–drain electrodes defining the channel length (scale bar = 1.5 μm).

making any charge correction unnecessary. However, for the sake of consistency of curve fitting analysis, the spectra were corrected by setting the main component of the C 1s peak at 284.8 eV. The XPS spectra were analyzed by CasaXPS software version 2.3.15. Curve fitting was performed after linear and Shirley background subtraction assuming Gaussian–Lorentzian line shape.

The curve fitting of the various core levels allowed us to calculate the elemental composition of the near-surface regions. The results are shown in Table 1. The calculations were done after intensity correction for Scoefield relative sensitivity factors and for an elastic mean free path (EMFP) assuming homogeneous distribution of the elements within the near-surface region. The results in Table 1 support the inferences given for the figures of the core levels. The relatively high C percentages indicate molecular attachment in ODT-treated samples. In addition, the larger relative amount of S (with respect to that in the unpassivated sample) indicates molecular attachment to the nanowire surface. Also, trace contaminant elements including Zn, Cl, and Na were only observed in the passivated samples and thus indicate such contaminants are artifacts of molecular deposition. The Si is a feature of the SiO_2/Si growth substrate.

High-resolution scans of the core levels give information on surface properties of each sample. The In 3d level is indicative of the In_2O_3 nanowires, while S 2p and S 2s levels give information on ODT molecular attachment on the nanowires. Figure 2a,b shows the In 3d core level spectra obtained from representative

TABLE 1. Surface Elemental Compositions (%) of Unpassivated (Sample 1) and ODT-Passivated (Sample 2) In_2O_3 Nanowires Measured by XPS at Photoemission Angle = 0°

	C	In	O	S	Si	Zn	Cl	Na
sample 1	13.5	0.5	15.8	0.0	70.2	0.0	0.0	0.0
sample 2	44.0	2.3	32.0	4.3	14.7	0.8	0.8	1.1

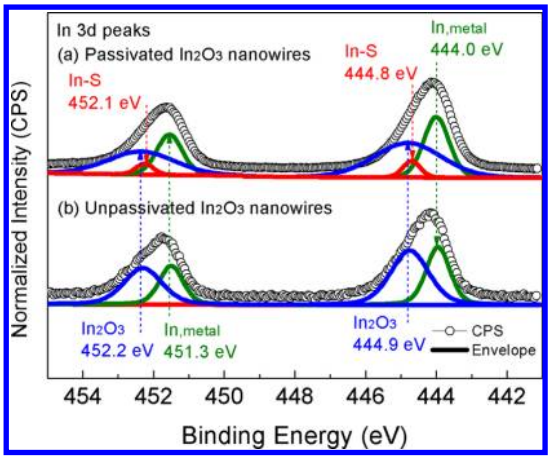

Figure 2. XPS spectra showing In 3d peaks for (a) ODT-passivated and (b) unpassivated In_2O_3 nanowires.

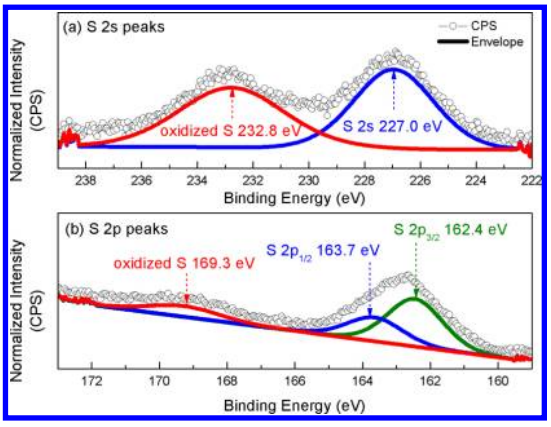

Figure 3. (a) S 2s and (b) S 2p spectra obtained from ODT-treated In_2O_3 nanowires.

ODT-passivated and unpassivated In_2O_3 nanowires, respectively. The In $3d_{5/2}$ peaks before and after ODT passivation were fitted with a main component peak (metallic In) at 444.0 eV and an oxide peak at 444.9 eV. Both peaks had accompanying In $3d_{3/2}$ doublet components at a separation of 7.3 eV and at an intensity ratio of 0.667, giving the main In $3d_{3/2}$ component a peak position of 451.3 eV and the oxide a peak position at 452.2 eV. However, only in the spectra of ODT-passivated nanowires could a component peak at 444.8 eV with doublet separation of 7.3 eV be fitted. This peak position corresponds to the In−S bond signature expected from ODT molecular attachment as described in the literature.[25]

Figure 3a,b shows the S 2s and S 2p spectra obtained from ODT-passivated In_2O_3 nanowires. The S 2p and S 1s signatures were registered only in samples where molecular deposition was performed. As depicted in Figure 3a, the S $2p_{3/2}$ peak was found at 162.4 eV, which corresponds to the sulfur covalently bound to the In_2O_3 nanowires. The S $2p_{1/2}$ component was fitted at a doublet separation of 1.3 eV and an intensity ratio of 0.5, which refers to the unbound sulfur. Oxidized S peak at 169.3 eV was also observed, which corresponds to the S−O bonds. In Figure 3b, the S 2s peak is seen at 227.0 eV while its oxidized component is shown at 232.8 eV. On the basis of the XPS analysis, we conclude that the ODT molecules are bound to the In_2O_3 nanowires through the thiol linkages.

In order to investigate the effects of the ODT passivation, electrical characterization was performed on the In_2O_3 NWTs before and after molecular deposition. Figure 4a,b shows the measured drain current *versus* gate−source voltage ($I_{ds}-V_{gs}$) characteristics at V_{ds} = 0.5 V for a representative In_2O_3 NWT before (circle) and after (triangle) ODT passivation in log and linear scale, respectively. The devices exhibit electrical characteristics of typical enhancement-mode n-type transistors. Note that the $I-V$ curves of NWTs with and without ODT passivation in Figure 4 are obtained from the devices fabricated using the above-mentioned optimization techniques; oxygen plasma, ozone, and laser annealing treatment (Figure 1). On the basis of recent NWT studies, such treatments further enhance device performance, especially in terms of I_{on}, I_{on}/I_{off}, SS, and μ_{eff} along with permanent positive shift in V_{th}.[11,23,24] The $I_{ds}-V_{gs}$ curve of a representative In_2O_3 NWT without optimization treatment (as-fabricated; square) is shown in Figure 4a as a reference. The as-fabricated In_2O_3 NWT shows I_{on} = 0.9 μA, $I_{on}/I_{off} = 9.14 \times 10^2$, SS = 750 mV/dec, μ_{eff} = 75 $cm^2/V\cdot s$, and V_{th} = −0.3 V; whereas the In_2O_3 NWT treated with oxygen plasma, ozone, and laser annealing (however, no passivation of the channel) exhibit increased I_{on} = 6.0 μA, improved $I_{on}/I_{off} = 10^6$, reduced SS = 230 mV/dec, increased μ_{eff} = 613 $cm^2/V\cdot s$, and positively shifted V_{th} = 0.3 V. After ODT passivation of the NWTs, device performance further improves to exhibit SS = 64 mV/dec, $I_{on}/I_{off} = 10^6$, μ_{eff} = 624 $cm^2/V\cdot s$, and V_{th} = 0.6 V. Following ODT passivation, the I_{on} for small $V_{gs}-V_{th}$ is smaller than that of the unpassivated devices. However, the I_{on} becomes comparable to that of unpassivated devices for larger $V_{gs}-V_{th}$. The drain current *versus* drain−source voltage ($I_{ds}-V_{ds}$) characteristics of the corresponding NWT before and after passivation are shown in Figure 4c,d, respectively. The single In_2O_3 NWTs exhibit high I_{on} near ∼40 μA at V_{ds} = 3.0 V prior to (43.3 μA at $V_{gs}-V_{th}$ = 3.7 V) and after (44.6 μA at $V_{gs}-V_{th}$ = 3.9 V) molecular passivation. The log scale $I_{ds}-V_{gs}$ curves of three representative NWTs before and after ODT passivation are shown in Figure 4e. Three devices exhibit average SS of 66 mV/dec (220 mV/dec) and V_{th} of 0.6 V (0.4 V) after (before) ODT passivation. Compared to TFTs based on α-Si, poly-Si, organic, TCO thin films, single-walled carbon nanotubes (SWCNTs), and oxide nanowires, the ODT-passivated In_2O_3 NWTs presented in this study show steep SS (∼64 mV/dec close to the thermionic emission limit of 60 mV/dec), low power (V_{th} near zero), and high-performance (high I_{on} and μ_{eff}) characteristics.[11,12,26−36] The obtained SS of 64 mV/dec is among the lowest value reported in In_2O_3-based TFTs and NWTs.[11,50]

The use of 1/*f* noise as a defect characterization method has become popular in recent years with the device scaling and emergence of nanoscale transistors.[37−39] In this study, 1/*f* noise in single In_2O_3 NWTs was measured in order to understand the effect of ODT molecules to the surface states of the NWTs, as shown in Figure 5. The drain bias was 0.5 V, and the frequency (*f*) range was varied from 1 Hz to 1.6 kHz. According to Hooge's empirical model, the 1/*f* noise behavior can be described by[40]

$$\frac{S_I(f)}{I_{ds}^2} = \frac{\alpha_H}{Nf^\beta} \quad (1)$$

where S_I is the current noise power spectrum density,

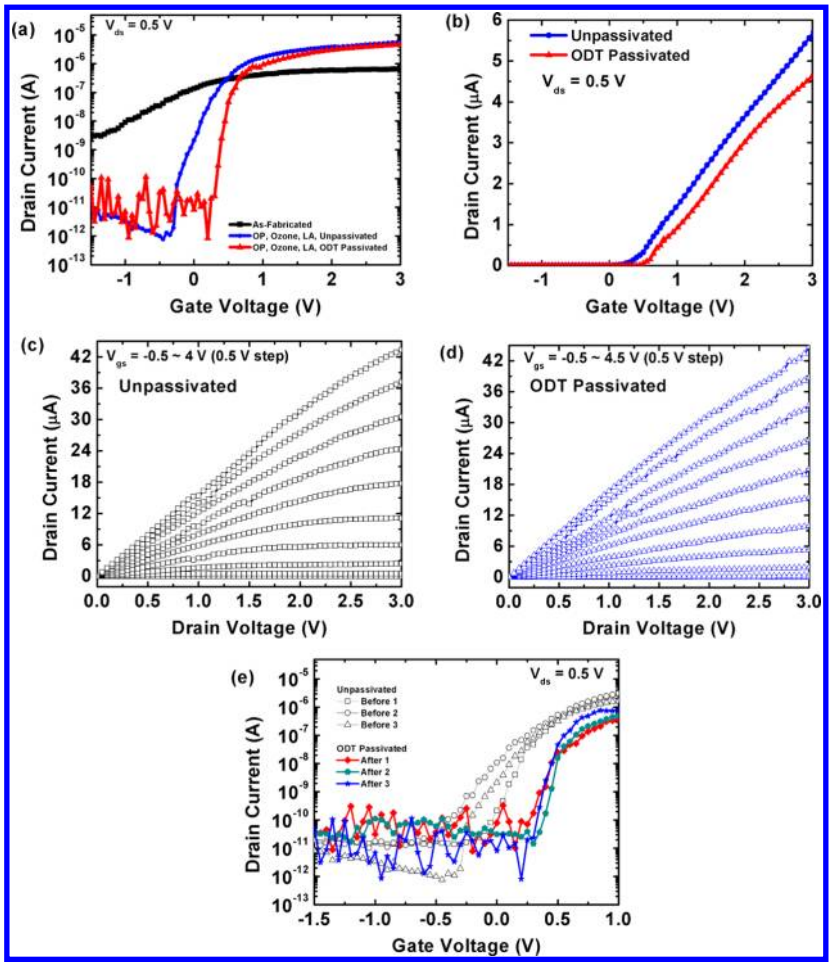

Figure 4. Measured current−voltage relationships of transistors fabricated under different conditions. For all cases except the as-fabricated state denoted in (a), 2 min ozone treatment at the channel region along with 60 s oxygen plasma (OP) cleaning and femtosecond laser annealing (LA) with laser fluence of 0.60 J/cm^2 at the contact region is used for device optimization. The (a) log scale and (b) linear scale of $I_{ds}-V_{gs}$ characteristics for representative In_2O_3 nanowire transistors before (circle) and after (triangle) ODT passivation at V_{ds} = 0.5 V. Note that $I_{ds}-V_{gs}$ of a representative as-fabricated device (square) is shown in (a) as a reference. The $I_{ds}-V_{ds}$ characteristics (c) before and (d) after ODT passivation are shown. (e) $I_{ds}-V_{gs}$ curves of three representative In_2O_3 nanowire transistors before (open) and after (solid) ODT passivation at V_{ds} = 0.5 V.

I_{ds} the drain to source current, α_H the Hooge's constant, N the total number of carriers in the nanowire channel, and β the frequency exponent which is ideally close to unity. The number of carriers in the case of strong inversion or strong accumulation is given by the equation

$$N = \frac{L_{ch}C_i(V_{gs} - V_{th})}{q} \quad (2)$$

Here, L_{ch} is the channel length, C_i the gate-to-channel capacitance, and q the electronic charge. Figure 5a shows the representative noise spectra (S_I/I_{ds}^2) of a single In_2O_3 NWT biased at $V_{gs}-V_{th}$ = 1.5 V prior to and after ODT passivation. In the 1/f region, S_I normalized by I_{ds}^2 varies as $f^{-\beta}$, where exponent β ranges between 0.91 and 1.15 from a linear fit of the spectrum. As shown in Figure 5a, the normalized 1/f noise spectrum of the unpassivated NWT is reduced by ~70% following ODT passivation. Combining eqs 1 and 2, S_I in strong on-state (when V_{gs} exeeds V_{ds}) can be expressed as

$$S_I = \frac{\alpha_H I_{ds}^2}{Nf} = \frac{q\alpha_H}{C_i f}\frac{I_{ds}^2}{|V_{gs} - V_{th}|} \quad (3)$$

Figure 5b,c shows the normalized square of the drain current ($I_{ds}^2/|V_{gs}-V_{th}|$) and S_I (at f = 100 Hz) *versus* the gate voltage before and after ODT passivation, respectively. The gate bias dependence of the S_I is in excellent agreement with the $I_{ds}^2/|V_{gs}-V_{th}|$ obtained from the experimental data, which are shown in thermionic emission dominated devices.[41] On the basis of the gate dependence of the 1/f noise amplitude and eq 3, α_H values are estimated as 1.82×10^{-2} and 7.41×10^{-3} for unpassivated and ODT-passivated NWTs, respectively. Broadly, one would expect α_H to be proportional to the interface density within the relevant energy range. The reduction of α_H following ODT treatment shows that the ODT on the nanowire channel is passivating the surface states, reducing the

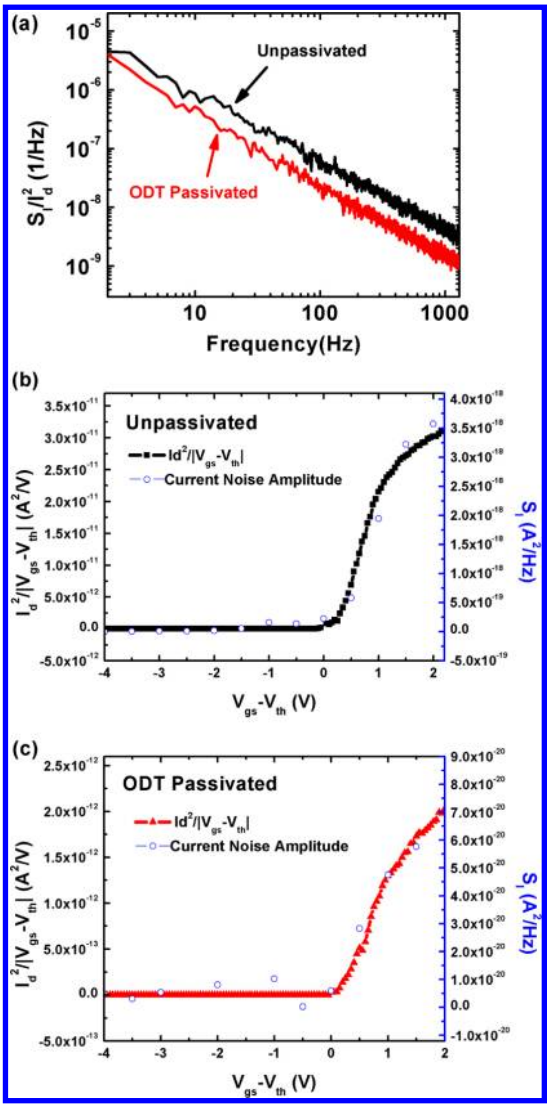

Figure 5. (a) Normalized current noise amplitude as a function of frequency for $V_{gs}-V_{th}$ = 1.5 V and V_{ds} = 0.5 V before and after ODT passivation. Measured $I_{ds}^2/|V_{gs}-V_{th}|$ and the amplitude of current noise spectrum (at 100 Hz) are plotted as a function of gate bias (b) before and (c) after ODT passivation for a fixed drain bias of 0.5 V.

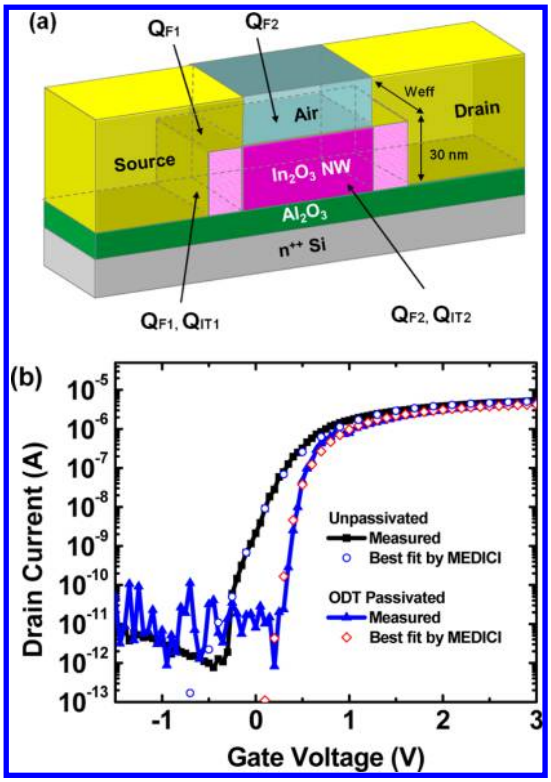

Figure 6. (a) In_2O_3 nanowire transistor structure for MEDICI simulation, using rectangular geometry to approximate cylindrical nanowire region. The nanowire is divided into two regions, the region covered by the source and drain electrodes (dashed) and the region exposed to air defining the channel. (b) Transfer characteristics ($I_{ds}-V_{gs}$) at V_{ds} = 0.5 V from experimental data and best-fit MEDICI simulations before and after ODT passivation are shown.

interface trap densities and modifying the fixed charge densities.

The improvement of device performance metrics such as steeper SS values and positively shifted V_{th} values after ODT passivation can be attributed to the effective change of surface state density on the nanowire. To quantitatively estimate the shift in surface state density upon ODT passivation, we used the MEDICI semiconductor device simulation software to relate the change of device performance after ODT deposition to nanowire interface trap states and fixed surface charges. The cross section of the simulated device structure is shown in Figure 6a. We used the same material parameters and layer thickness as the fabricated NWTs. Since the MEDICI simulation is a 2D simulation, the overall geometry of the nanowire device can be approximated by utilizing an effective width (W_{eff}) of 60 nm, determined by equating the capacitance predicted by MEDICI (capacitance per unit width times W_{eff}) with the cylinder-on-plate capacitance mode and providing the correct I_{on}. The calculated W_{eff} is larger than the nanowire diameter presumably due to the fringing effects, which are not considered in the 2D MEDICI simulation. In the simulation, the *n*-branch of the experimental data (electrons) is taken into account. In the nanowire device structure, we used fixed negative charge densities at the top and bottom interfaces of the nanowire at the contacts (Q_{F1}) and the channel (Q_{F2}) and voltage-variable interfacial trap densities at the $Al_2O_3-In_2O_3$ interface at the contacts (Q_{IT1}) and the channel (Q_{IT2}), as shown in Figure 6a.

As shown in Figure 6b, a series of simulations were performed using Q_{F1}, Q_{F2}, Q_{IT1}, and Q_{IT2} as parameters to fit the experimental transfer curve ($I_{ds}-V_{gs}$) data from both unpassivated (squares) and ODT-passivated (triangles) devices. The best-fit parameters are summarized in Table 2. In order to directly compare effects of modifications to the channel region, the values of Q_{F1} and Q_{IT1} obtained from fitting the data from the

TABLE 2. Best-Fit Parameter Values Obtained from the MEDICI Simulation for Unpassivated and ODT-Passivated In_2O_3 Nanowire Transistors

	Q_{IT1} (cm^{-2} eV^{-1})	Q_{F1} (cm^{-2})	Q_{IT2} (cm^{-2} eV^{-1})	Q_{F2} (cm^{-2})
unpassivated	4.3×10^{12}	-3×10^{10}	4.3×10^{12}	-3×10^{10}
ODT-passivated	4.3×10^{12}	-3×10^{10}	1.2×10^{11}	-4×10^{10}

unpassivated device were used in the modeling of the passivated device. The reduction of Q_{IT2} following ODT deposition is presumably due to the thiol linkage at the nanowire surface as evidenced in the XPS data. Although net charge is not expected to be induced by the ODT, In−S and/or O−S bonding is likely to induce a fixed charge dipole which can result in the significant change of Q_{F2} in the numerical model. The 1 order of magnitude reduction in Q_{IT2} appears to be the primary mechanism responsible for the significant decrease in SS values following ODT passivation. The increased number of Q_{F2} at the ODT-passivated nanowire is also expected to contribute to improved SS characteristics since the negative charges located at the nanowire surface are known to deplete the nanowire body, consequently reducing the voltage required to switch between on- and off-state and positively shifting the V_{th}. Also, the shift of Q_{F2} in the model yields a good fit to the gradual increase in on-current for small $V_{gs}-V_{th}$. The increased number of negative fixed charges upon ODT deposition is expected to decrease the effective doping density not only at the channel but also near the contacts, resulting in more gradual band bending at the space charge region, leading to a less transparent contact for low V_{gs} near V_{th}.

Along with the MEDICI simulation, the interface trap density (Q_{IT}) can also be calculated from the measured SS and 1/*f* noise amplitude. While SS is well-known to provide information about the interface quality especially related in subthreshold regime, it has been reported that the 1/*f* noise is more related with the Q_{IT} near the Fermi level.[46] In order to study the effect of ODT passivation on both the subthreshold and on-state operation of NWTs, the Q_{IT} values were extracted both from SS and 1/*f* noise measurement and compared to the MEDICI simulation results. In the long-channel device, the subthreshold swing can be expressed as[45]

$$SS = (\ln 10)\left(\frac{kT}{q}\right)\left(1+\frac{C_{dep}+C_{IT}}{C_{ox}}\right) \quad (4)$$

Here, *k* is Boltzmann's constant, *T* (=300 K) the temperature, C_{dep} the depletion layer capacitance, which is near zero for fully depleted nanowires, C_{IT} the capacitance associated with the interface trap density (Q_{IT}), and C_{ox} oxide capacitance in F/cm^2 units. The relation between C_{IT} and Q_{IT} is defined by the equation $C_{IT} = q^2 Q_{IT}$, and when combined with eq 4, Q_{IT} can be

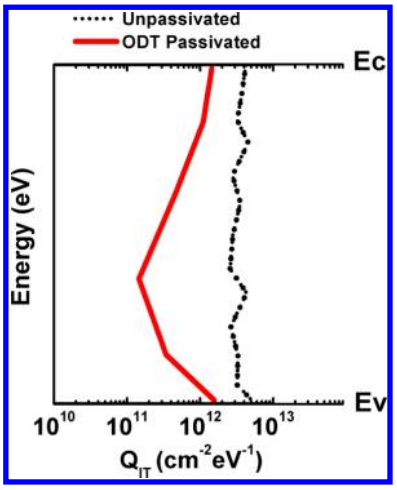

Figure 7. Trap energy distribution inferred from subthreshold $I_{ds}-V_{ds}$ curves before and after passivation.

extracted using

$$Q_{IT} = \frac{C_{IT}}{q^2} = \frac{1}{q^2}C_{ox}\left(\frac{SS}{(\ln 10)\left(\frac{kT}{q}\right)} - 1\right) \quad (5)$$

From eq 5 and the average SS = 64 mV/dec (230 mV/dec) measured from $I_{ds}-V_{gs}$ curves of Figure 4a, Q_{IT} of 1.19×10^{11}/$cm^2 \cdot$eV (4.15×10^{12}/$cm^2 \cdot$eV) is estimated for ODT-passivated (unpassivated) devices, respectively. Note that the Q_{IT} extracted from eq 5 is in good agreement with the values extracted from the MEDICI simulations.

Assuming that carrier number fluctuation is the only mechanism responsible for the 1/*f* noise, the S_I normalized by I_{ds}^2 can be expressed as[46]

$$\frac{S_I}{I_{ds}^2} = \left(\frac{1}{N}\right)^2 \frac{kT}{f\gamma d_{nw} L_{ch}} N_{IT}(E_F) \quad (6)$$

where γ is the attenuation coefficient of the electron wave function in the oxide, d_{nw} is the nanowire diameter, and $N_{IT}(E_F)$ is the interface trap density at the quasi-Fermi level (E_F) in units of /cm^3 eV. The WKB theory for carrier tunneling defines γ by the equation[47]

$$\gamma = \frac{4\pi}{h}\sqrt{2m^*\Phi_{TB}} \quad (7)$$

where *h* is Planck's constant, *m** is the effective mass of the carrier in oxide, and Φ_{TB} the tunneling barrier height seen by the carriers at the interface. Using eqs 6 and 7 and S_I/I_{ds}^2 values at *f* = 100 Hz obtained from noise spectra shown in Figure 5a, Q_{IT} values of 1.33×10^{12} and 4.08×10^{12}/$cm^2 \cdot$eV are calculated for ODT-passivated and unpassivated NWTs, respectively. For unpassivated devices, Q_{IT} obtained from S_I/I_{ds}^2 agrees well with the value obtained from SS (or MEDICI simulation). For ODT-passivated devices, however, Q_{IT}

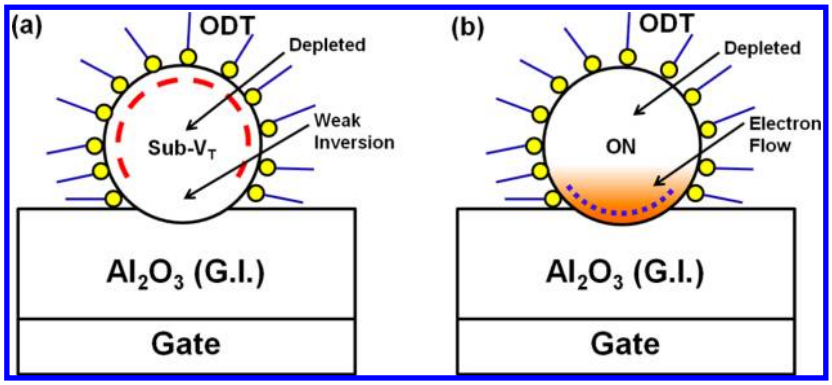

Figure 8. Spatial location of the electron channel of the ODT-passivated NWTs at the (a) subthreshold and (b) on-state region.

extracted from the noise power is 1 order of magnitude higher than the value obtained from the subthreshold $I-V$ characteristics.

The discrepancy of Q_{IT} extracted from the noise measurement and the subthreshold $I-V$ relation can be explained by (i) the trap energy distribution at the band gap and/or (ii) the spatial location of the electron channel. The energy (E) and gate voltage relation can be expressed as

$$dE = dV_{gs}\left(\frac{C_{ox}}{C_{ox}+C_{dep}+C_{IT}}\right) \quad (8)$$

from the voltage divider model of capacitors connected in parallel. The distribution of Q_{IT} *versus* E throughout the band gap can be extracted from instantaneous SS at the corresponding V_{gs} before and after ODT passivation combined with eqs 6 and 8 as plotted in Figure 7.[45] Note that the Q_{IT} of 4.1 $\times$ 10^{12}/cm^2·eV is uniformly distributed throughout the band gap prior to passivation. Following ODT passivation, however, a non-uniform distribution of trap density is observed; the Q_{IT} is 1.4 $\times$ 10^{12}/cm^2·eV, similar to the value extracted from noise measurements, near the conduction band region, but 1 order of magnitude lower ($\sim$1.3 $\times$ 10^{11}/cm^2·eV) near midgap, close to the value obtained from SS. Note that the noise measurements are performed at bias points corresponding to a Fermi energy near the conduction band (E_c); at this point, the difference in Q_{IT} for passivated *versus* unpassivated is relatively small. The structure of the NWTs can be simplified as a cylindrical nanowire placed on top of a dielectric plate as shown in Figure 8a,b. The Al_2O_3 has a permittivity about nine times higher than the atmosphere; therefore, the current density through the cylindrical nanowire should be higher near the nanowire to dielectric interface than the surface around the nanowire body. Furthermore, it has been reported that conduction through In_2O_3 nanowire is surface-centered rather than bulk-centered because oxygen vacancies at the nanowire surface have a significant impact on the electron transport through In_2O_3 nanowires.[13] As the enhancement-mode devices in the current study are back-gated, the inversion layer is expected to form near the bottom of the nanowire near the gate insulator as V_{gs} increases above V_{th}, entering the device turn-on regime as depicted in Figure 8b. As ODT passivation was performed after the nanowire channel is placed on top of the gate insulator, the quality of the interface between the nanowire and the thin Al_2O_3 layer (dot) is expected to dominate the lower limit of the noise power spectrum in the strong inversion regime. For operation in the subthreshold region, the quality of the ODT-passivated nanowire surface (dash) rather than the $Al_2O_3-In_2O_3$ nanowire interface is expected to play a major role, as shown in Figure 8a, resulting in dramatically reduced SS close to the thermionic emission limit of $\sim$60 mV/dec following ODT passivation. This is consistent with the value of $\alpha_H \sim 7.41 \times 10^{-3}$ (ODT-passivated In_2O_3 NWTs) which is comparable to the prior reported values for ZnO, SnO_2, and CNT-based FETs using ALD-deposited Al_2O_3 as the back-gate insulator in ambient, which exhibit much larger SS compared to our study.[41,48,49]

CONCLUSION

In conclusion, ODT treatment of the In_2O_3 nanowire transistor channel is effective in passivating the surface states and significantly improving the SS values. We demonstrate that ODT passivation can reduce the SS to $\sim$64 mV/dec. XPS studies of the ODT-passivated nanowires indicate that ODT molecules are bound to In_2O_3 nanowires through the thiol linkages. The 1/f noise measurements indicate that the noise spectra density is reduced after the ODT passivation of the nanowire channel region. MEDICI simulation allows quantification of the effects of ODT passivation in terms of reducing the interface trap charge states and modifying the fixed charges at the nanowire interface. The comparison of Q_{IT} values extracted from both subthreshold $I-V$ characteristics and 1/f noise measurements before and after ODT passivation give

physical insights in realizing low-noise electronics based on nanowires. This study reports that ODT passivation is a promising optimization technology for the realization of low-power and fast-switching circuits that is applicable to CMOS logic or memory/display circuitry.

METHODS

Fabrication of In_2O_3 NWT Devices. The NWTs are fabricated on a heavily doped n-type Si substrates (ρ = 0.01 Ω·cm) with a thermally grown 500 nm SiO_2 layer. Channel regions were defined by photolithographic patterning followed by etching in BOE to remove the oxide. A 30 nm thick layer of Al_2O_3 gate dielectric (dielectric constant (ε_{ox}) ~9, capacitance ~600 nF/cm^2, electrical breakdown field ~8 MV/cm) was then deposited by atomic layer deposition (ALD) at 300 °C using an ASM Microchemistry F-120 ALCVD reactor and subsequently annealed in N_2 at 600 °C for 30 s. The thin high-k gate dielectric allows the channel potential to be modulated at a relatively low gate voltage without significant gate leakage. Single-crystalline In_2O_3 nanowires (doping concentration (N_D) ~1.2×10^{16} cm^{-3}) with diameters of 20−30 nm and lengths of 5−10 μm were grown by pulsed laser ablation method on oxidized Si substrates coated with 2 nm thick gold thin film as the catalyst.[22] Note that the nanowire diameter is similar to the Debye length (L_D) of ~25 nm ($L_D = (\varepsilon_o \varepsilon_{nw} kT/q^2/N_D)^{1/2}$), and therefore, the interface state density is expected to play a significant role in the electron transport and the scattering at the nanowire channel. The nanowires were suspended in VLSI-grade isopropyl alcohol solution and then dispersed onto the patterned device substrates. Finally, the source−drain electrodes were formed by electron beam deposition of Al at ~5×10^{-7} Torr (thickness = 110 nm, deposition rate = 0.1 Å/s) followed by a lift-off process, with the spacing between contacts (1.5−2 μm) defining the channel length (L_{ch}).

Optimization Techniques. An oxygen plasma treatment system (pressure = 10 mTorr, power = 100 W, time = 60 s, and volume flow rates of oxygen = 150 sccm) was used to selectively expose the nanowire region at the contacts. Ozone treatment (UV-ozone cleaner, UVO 342, Jelight) was performed at the nanowire channel for 2 min. The ozone environment was obtained using an oxygen concentration of 50 ppm, an ultraviolet (UV) wavelength of 184.9 nm, and UV lamp power of 28 mW cm^{-2} at 254 nm. Note that when the devices were exposed to oxygen plasma and ozone, they were shielded from UV light. A commercial amplified femtosecond laser system from Spectra-Physics (Ti:sapphire laser pulse width = 50 fs centered at 800 nm, laser fluence = 0.60 J/cm^2, repetition rate = 1 kHz, scan speed = 1 μm/s, objective lens = 100×, NA 0.8, and beam diameter = 1.22 μm) was used to selectively anneal the contact regions of the NWTs. A high-precision, three-axis computer-controlled positioning stage was used to move the sample with respect to the laser beam.

Characterization Methodology. Room-temperature $I-V$ measurements were performed using an HP 4156A semiconductor parameter analyzer. Flicker noise characteristics were measured in ambient using a SR 570 low-noise current preamplifier and a HP 3561A dynamic signal analyzer. The nanowires within a device were imaged with a Hitachi S-4800 FE-SEM following electrical characterization.

Calculation of Mobility and Threshold Voltage. The field-effect mobility ($\mu_{eff} = dI_{ds}/dV_{gs} \times L_{ch}^2/C_i \times 1/V_{ds}$) was extracted from $I-V$ characteristics at V_{ds} = 0.5 V, using the calculated gate-to-channel capacitance $C_i = 2\pi\varepsilon_0 k_{eff}/\cosh^{-1}(1 + t_{ox}/r_{nw})$, which represents a cylinder-on-plate model. Here, $k_{eff} \sim 9$ is the effective dielectric constant of the ALD Al_2O_3, $L_{ch} \sim 2$ μm is the device channel length, and the $r_{nw} \sim 15$ nm is the nanowire radius. The threshold voltage was obtained by extrapolating the linear portion of the $I_{ds}-V_{gs}$ to zero drain current curves from the maximum slope where the transconductance ($g_m = dI_{ds}/dV_{gs}$) is maximal.

Material Parameter and Layer Thickness for Simulation. The nanowire channel was modeled as a film of In_2O_3 with nanowire thickness of physical diameter of the nanowire (d_{nw} = 30 nm), channel length (L_{ch}) of 2 μm, relative dielectric constant (ε_{nw}) of 8.9, electron affinity 3.7 eV, energy band gap 2.6 eV, conduction band effective density of states 4.12×10^{18}/cm^3, and valence band effective density of states 1.16×10^{19}/cm^3.[22,23] ALD-deposited Al_2O_3 film was defined as an insulator with dielectric constant (ε_{ox}) of 9.0 and oxide thickness (d_{ox}) of 30 nm. In_2O_3 nanowire doping concentration (N_D) was set as 1.2×10^{16} cm^{-3} within the channel region which corresponds to the n-type properties of the nanowires synthesized by the laser ablation method.[22,23] The characteristic length ($\lambda = (\varepsilon_{nw}/\varepsilon_{ox} \times d_{nw} \times d_{ox})^{1/2}$) over which the bands bend at the metal-semiconductor (M-S) contact interface was calculated to be 25 nm.[42] In the MEDICI simulation, an effective doping concentration was used within the band-bending region at the metal−nanowire interface, in order to provide band bending over a length comparable to λ. An effective concentration of 6.5×10^{16} cm^{-3} for as-fabricated devices was extracted by approximately equating the potential distribution at the metal−nanowire junction near the dielectric interface to the potential distribution within a uniformly doped Schottky barrier.[43,44]

Conflict of Interest: The authors declare no competing financial interest.

Acknowledgment. We acknowledge P. Srisungsitthisunti and X. Xu at Purdue University for assistance with the femtosecond laser annealing. This research was supported by the National Science Foundation (ECCS 1118934). This research was also partially supported by the National Research Foundation of Korea (NRF) funded by the Ministry of Education, Science and Technology (2011K000627).

REFERENCES AND NOTES

1. Lieber, C. M. Nanoscale Science and Technology: Building a Big Future from Small Things. *MRS Bull.* **2003**, *28*, 486.
2. Cao, Q.; Kim, H.; Pimparkar, N; Kulkarni, J. P.; Wang, C.; Shim, M.; Roy, K.; Alam, M. A.; Rogers, J. A. Medium-Scale Carbon Nanotube Thin-Film Integrated Circuits on Flexible Plastic Substrates. *Nature* **2008**, *454*, 495–500.
3. Lao, J.; Wen, J.; Ren, Z. Hierarchical ZnO Nanostructures. *Nano Lett.* **2002**, *2*, 1287–1291.
4. Choopun, S.; Vispute, R.; Noch, W.; Balsamo, A.; Sharma, R.; Venkatesan, T.; Iliadis, A.; Look, D. Oxygen Pressure-Tuned Epitaxy and Optoelectronic Properties of Laser-Deposited ZnO Films on Sapphire. *Appl. Phys. Lett.* **1999**, *75*, 3947–3949.
5. Ju, S.; Lee, K.; Yoon, M. H.; Facchetti, A.; Marks, T. J.; Janes, D. B. High Performance ZnO Nanowire Field Effect Transistors with Organic Gate Nanodielectrics: Effects of Metal Contacts and Ozone Treatment. *Nanotechnology* **2007**, *18*, 155201.
6. Zhang, D.; Liu, Z.; Li, C.; Tang, T.; Liu, X.; Han, S.; Lei, B.; Zhou, C. Detection of NO_2 Down to ppb Levels Using Individual and Multiple In_2O_3 Nanowire Devices. *Nano Lett.* **2004**, *4*, 1919–1924.
7. Screenivas, K.; Rao, T. S.; Mansingh, A. Preparation and Characterization of RF Sputtered Indium Tin Oxide Flms. *J. Appl. Phys.* **1985**, *57*, 384.
8. Liess, M. Electric-Field-Induced Migration of Chemisorbed Gas Molecules on a Sensitive Film—A New Chemical Sensor. *Thin Solid Films* **2002**, *410*, 183.
9. Curreli, M.; Li, C.; Sun, Y.; Lei, B.; Gundersen, M. A.; Thompson, M. E.; Zhou, C. Selective Functionalization of In_2O_3 Nanowire Mat Devices for Biosensing Applications. *J. Am. Chem. Soc.* **2005**, *127*, 6922–6923.
10. Shigesato, Y.; Takaki, S.; Haranoh, T. Electrical and Structural Properties of Low Resistivity Tin-Doped Indium Oxide Films. *J. Appl. Phys.* **1992**, *71*, 3356.

11. Ju, S.; Facchetti, A.; Xuan, Y.; Liu, J.; Ishikawa, F.; Ye, P.; Zhou, C.; Marks, T. J.; Janes, D. B. Fabrication of Fully Transparent Nanowire Transistors for Transparent and Flexible Electronics. *Nat. Nanotechnol.* **2007**, *2*, 378–384.
12. Ju, S.; Li, J.; Liu, J.; Chen, P.-C.; Ha, Y.-G.; Ishikawa, F.; Chang, H.; Zhou, C.; Facchetti, A.; Janes, D. B.; *et al.* Transparent Active Matrix Organic Light-Emitting Diode Displays Driven by Nanowire Transistor Circuitry. *Nano Lett.* **2008**, *8*, 997–1004.
13. Kolmakov, A.; Moskovits, M. Chemical Sensing and Catalysis by One-Dimensional Metal-Oxide Nanostructures. *Annu. Rev. Mater. Res.* **2004**, *34*, 151–180.
14. King, P. D. C.; Veal, T. D.; Payne, D. J.; Bourlange, A.; Egdell, R. G.; McConville, C. F. Surface Electron Accumulation and the Charge Neutrality Level in In_2O_3. *Phys. Rev. Lett.* **2008**, *101*, 116808.
15. Zhang, D.; Li, C.; Han, S.; Liu, X.; Tang, T.; Jin, W.; Zhou, C. Ultraviolet Photodetection Properties of Indium Oxide Nanowires. *Appl. Phys. A: Mater. Sci. Process.* **2003**, *77*, 163–166.
16. Zhang, D.; Li, C.; Liu, X.; Han, S.; Tang, T.; Zhou, C. Doping Dependent NH Sensing of Indium Oxide Nanowires. *Appl. Phys. Lett.* **2003**, *83*, 1845.
17. Moon, T.; Jeong, M.; Oh, B.; Ham, M.; Jeun, M.; Lee, W.; Myoung, J. Chemical Surface Passivation of HfO_2 Films in a ZnO Nanowire Transistor. *Nanotechnology* **2007**, *17*, 2116–2121.
18. Song, S.; Hong, W.; Kwon, S.; Lee, T. Passivation Effects on ZnO Nanowire Field Effect Transistors under Oxygen Ambient, and Vacuum Environments. *Appl. Phys. Lett.* **2008**, *92*, 263109.
19. Li, C.; Fan, W.; Lei, B.; Zhang, D.; Han, S.; Tang, T.; Liu, X.; Liu, Z.; Asano, S.; Meyyappan, M.; *et al.* Multilevel Memory Based on Molecular Devices. *Appl. Phys. Lett.* **2004**, *84*, 1949.
20. Duan, X.; Huang, Y.; Lieber, C. M. Nonvolatile Memory and Programmable Logic from Molecule-Gated Nanowires. *Nano Lett.* **2002**, *2*, 487–490.
21. Hau, S. K.; Yip, H.; Chen, K.; Zou, J.; Jen, A. K. Y. Solution Processed Inverted Tandem Polymer Solar Cells with Self-Assembled Monolayer Modified Interfacial Layers. *Appl. Phys. Lett.* **2010**, *97*, 253307.
22. Li, C.; Zhang, D.; Han, S.; Liu, X.; Tang, T.; Zhou, C. Diameter-Controlled Growth of Single-Crystalline In_2O_3 Nanowires and Their Electronic Properties. *Adv. Mater.* **2003**, *15*, 143–146.
23. Kim, S.; Delker, C.; Chen, P.; Zhou, C.; Ju, S.; Janes, D. B. Oxygen Plasma Exposure Effects on Indium Oxide Nanowire Transistors. *Nanotechnology* **2010**, *21*, 145207.
24. Kim, S.; Kim, S.; Srisungsitthisunti, P.; Lee, C.; Xu, M.; Ye, P. D.; Qi, M.; Xu, X.; Zhou, C.; Ju, S.; *et al.* Selective Contact Anneal Effects on Indium Oxide Nanowire Transistors Using Femtosecond Laser. *J. Phys. Chem. C* **2011**, *115*, 17147–17153.
25. Hang, Q.; Wang, F.; Carpenter, P. D.; Zemlyanov, D.; Zakharov, D.; Stach, E. A.; Buhro, W. E.; Janes, D. B. Role of Molecular Surface Passivation in Electrical Transport Properties of InAs Nanowires. *Nano Lett.* **2008**, *8*, 49–55.
26. Ucjikoga, S. Low-Temperature Polycrystalline Silicon Thin-Film Transistor Technologies for System-On Glass Displays. *MRS Bull.* **2002**, *27*, 881–886.
27. Madelung, O., Ed. *Technology and Applications of Amorphous Silicon*; Springer: Berlin, 2000.
28. Snell, A. J.; Mackenzie, K. D.; Spear, W. E.; LeComber, P. G.; Hughes, A. J. Application of Amorphous Silicon Field Effect Transistors in Addressable Liquid Crystal Display Panels. *Appl. Phys. A: Mater. Sci. Process.* **1981**, *24*, 357–362.
29. Gelinck, G. H.; Edzer, H.; Huitema, A.; van Veenendaal, E. V.; Cantatore, E.; Schrijnemakers, L; van der Putten, J. B. P. H.; Geuns, T. C. T.; Beenhakkers, M.; Giesbers, J. B.; *et al.* Flexible Active-Matrix Displays and Shift Registers Based on Solution-Processed Organic Transistors. *Nat. Mater.* **2004**, *3*, 106–110.
30. Klauk, H.; Halik, M.; Zschieschang, U.; Eder, F.; Rohde, D.; Schmid, G.; Dehm, C. Flexible Organic Complementary Circuits. *IEEE Trans. Electron Devices* **2005**, *52*, 618–622.
31. Hoffman, R. L.; Norris, B. J.; Wager, J. F. ZnO-Based Transparent Thin-Film Transistors. *Appl. Phys. Lett.* **2003**, *82*, 733–735.
32. Ueda, K.; Hase, T.; Yanagi, H.; Kawazoe, H.; Hosono, H.; Ohta, H.; Orita, M.; Hirano, M. Epitaxial Growth of Transparent p-Type Conducting $CuGaO_2$ Thin Films on Sapphire (001) Substrates by Pulsed Laser Deposition. *J. Appl. Phys.* **2001**, *89*, 1790–1793.
33. Inoue, S.; Ueda, K.; Hosono, H.; Hamada, N. Electronic Structure of the Transparent p-Type Semiconductor (LaO)CuS. *Phys. Rev. B* **2001**, *64*, 245211–245215.
34. Chiang, H. Q.; Hong, D.; Hung, C. M.; Presley, R. E.; Wager, J. F.; Park, C.-H.; Keszler, D. A.; Herman, G. S. Thin-Film Transistors with Amorphous Indium Gallium Oxide Channel Layers. *J. Vac. Sci. Technol., B* **2006**, *24*, 2702–2705.
35. Kim, S.; Kim, S.; Park, J.; Ju, S.; Mohammadi, S. Fully Transparent Pixel Circuits Driven by Random Network Carbon Nanotube Transistor Circuitry. *ACS Nano* **2010**, *4*, 2994–2998.
36. Chen, P.; Fu, Y.; Aminirad, R.; Wang, C.; Zhang, J.; Wang, K.; Galatsis, K.; Zhou, C. Fully Printed Separated Carbon Nanotube Thin Film Transistor Circuits and Its Application in Organic Light Emitting Diode Control. *Nano Lett.* **2011**, *11*, 5301–5308.
37. Tersoff, J. Low-Frequency Noise in Nanoscale Ballistic Transistors. *Nano Lett.* **2007**, *7*, 194–198.
38. Lin, Y.; Appenzeller, J.; Knock, J.; Chen, Z.; Avouris, P. Low-Frequency Current Fluctuations in Individual Semiconducting Single-Wall Carbon Nanotubes. *Nano Lett.* **2006**, *6*, 930–936.
39. Back, J. H.; Kim, S.; Mohammadi, S.; Shim, M. Low-Frequency Noise in Ambipolar Carbon Nanotube Transistors. *Nano Lett.* **2008**, *8*, 1090–1094.
40. Hooge, F. N. 1/*f* Noise Sources. *IEEE Trans. Electron Devices* **1994**, *41*, 1926–1935.
41. Ishigami, M.; Chen, J. H.; Williams, E. D.; Tobias, D.; Chen, Y. F.; Fuhrer, M. S. Hooge's Constant for Carbon Nanotube Field Effect Transistors. *Appl. Phys. Lett.* **2006**, *88*, 203116.
42. Yan, R. H.; Ourmazd, A.; Lee, K. F. Scaling the Si MOSFET: From Bulk to SOI to Bulk. *IEEE Trans. Electron Devices* **1992**, *39*, 1704–1710.
43. Padovani, F. A.; Stratton, R. Field and Thermionic-Field Emission in Schottky Barriers. *Solid-State Electron.* **1966**, *9*, 695.
44. Appenzeller, J.; Knoch, J.; Bjork, M. T.; Riel, H.; Schmid, H.; Riess, W. Toward Nanowire Electronics. *IEEE Trans. Electron Devices* **2008**, *55*, 11.
45. Sze, S. M.; Ng, K. K. *Physics of Semiconductor Devices*, 3rd ed.; Wiley: New York, 2007.
46. Hung, K. K.; Ko, P. K.; Hu, C.; Cheng, Y. C. A Unified Model for the Flicker Noise in Metal-Oxide-Semiconductor Field-Effect Transistors. *IEEE Trans. Electron Devices* **1990**, *37*, 654–665.
47. Christensson, S.; Lundstrom, I.; Svensson, C. Low Frequency Noise in MOS Transistors. *Solid-State Electron.* **1968**, *11*, 797.
48. Ju, S.; Kim, S.; Mohammadi, S.; Janes, D. B.; Ha, Y.-G.; Facchetti, A.; Marks, T. J. Interface Studies of ZnO Nanowire Transistors Using Low-Frequency Noise and Temperature-Dependent *I*−*V* Measurements. *Appl. Phys. Lett.* **2008**, *92*, 022104.
49. Ju, S.; Chen, P.; Zhou, C.; Ha, Y.-G.; Facchetti, A.; Marks, T. J.; Kim, S.; Mohammadi, S.; Janes, D. B. High Performance In_2O_3 Nanowire Transistors Using Organic Gate Nanodielectrics. *Appl. Phys. Lett.* **2008**, *92*, 243120.
50. Chen, P.; Shen, G.; Chen, H.; Ha, Y.; Wu, C.; Sukcharoenchoke, S.; Fu, Y.; Liu, J.; Facchetti, A.; Marks, T. J.; *et al.* High-Performance Single-Crystalline Arsenic-Doped Indium Oxide Nanowires for Transparent Thin-Film Transistors and Active Matrix Organic Light-Emitting Diode Displays. *ACS Nano* **2009**, *3*, 3383–3390.